ELSEVIER

Contents lists available at ScienceDirect

# Materials Science & Engineering C

journal homepage: www.elsevier.com/locate/msec





# Incorporation of 45S5 bioglass $\emph{via}$ sol-gel in $\beta$ -TCP scaffolds: Bioactivity and antimicrobial activity evaluation

B.R. Spirandeli <sup>a</sup>, R.G. Ribas <sup>b</sup>, S.S. Amaral <sup>c</sup>, E.F. Martins <sup>a</sup>, E. Esposito <sup>a</sup>, L.M.R. Vasconcellos <sup>c</sup>, T. M.B. Campos <sup>b</sup>, G.P. Thim <sup>b</sup>, E.S. Trichês <sup>a</sup>, <sup>\*</sup>

- <sup>a</sup> Federal University of São Paulo (UNIFESP), 330 Talim St, 12231-280 São José dos Campos, SP, Brazil
- <sup>b</sup> Technological Institute of Aeronautics (ITA), 50 Mal. Eduardo Gomes Plaza, 12228-900 São José dos Campos, SP, Brazil
- c São Paulo State University (UNESP), Institute of Science and Technology, 777 Eng. Francisco José Longo Avenue, 12245-000 São José dos Campos, SP, Brazil

#### ARTICLE INFO

#### Keywords: Scaffolds Tricalcium phosphate 45S5 bioglass Sol-gel Bioactivity Biocompatibility Antimicrobial activity

#### ABSTRACT

In this work, β-TCP (β-tricalcium phosphate) bioresorbable scaffolds were prepared by the gel casting method. Then, they were impregnated with a 45S5 bioglass sol gel solution to improve biocompatibility and promote bioactivity and antimicrobial activity. The β-TCP scaffolds had an apparent porosity of 72%, and after the incorporation of the bioglass, this porosity was maintained. The elements of the bioglass were incorporated into  $\beta$ -TCP matrix and there was a partial transformation from the  $\beta$ -TCP phase to the  $\alpha$ -TCP ( $\alpha$ -tricalcium phosphate) phase, besides the formation of bioactive calcium and sodium-calcium silicates. The scaffolds β-TCP with 45S5 bioglass incorporated (β-TCP/45S5) did not show a reduction in their values of mechanical strength and Weibull modulus, despite the partial transformation to the α-TCP phase. Bioactivity, cell viability, and antimicrobial activity improved significantly for the β-TCP/45S5 scaffold comparing to the scaffold without the bioglass. The mineralization of carbonated hydroxyapatite was verified in Simulated Body Fluid (SBF). The cell viability, cells, increased by 178%, and β-TCP/45S5 scaffold also enhanced cell activity and osteoblast differentiation observed by means of total protein contend and alkaline phosphatase activity, respectively. The formation of growth inhibition zones was also observed in the disk diffusion assay for three tested microorganisms: Staphylococcus aureus, Escherichia coli and Candida albicans. To conclude, the vacuum impregnation method in 45S5 bioglass sol gel solution was effective in penetrating all the interconnected macroporosity of the scaffolds and covering the surface of the struts, which improved their biological properties in vitro, bioactivity and antibacterial activity, without reducing mechanical strength and porosity values. Thus, the  $\beta$ -TCP/45S5 scaffolds are shown as potential candidates for use in tissue engineering, mainly in bone tissue regeneration and recovery.

#### 1. Introduction

Every day, damage resulting from trauma, disease or injury to bone tissues requires treatment systems that facilitate their repair, replacement, or regeneration. These systems are generally based on the transplantation of autografts or allografts to the injured site. However, this practice is laborious, painful, subject to infections, bruising, rejection, and introduction of diseases [1]. Thus, the use of bioceramics bone grafts has been an alternative for these treatment systems [2,3]. It is desirable that these grafts have biocompatibility, compatible mechanical resistance to the implantation site, bioactivity, bioresorbability and resistance to common microorganisms in surgical procedures for

implantation [3].

Bone grafts can be produced in the form of scaffolds. Scaffolds are three-dimensional porous supports that assist in tissue reconstitution, supporting and inducing cell proliferation and growth. Calcium phosphates (CaPs) are bioceramics widely used in the production of scaffolds for implantation and treatment of damage to bone tissue. The most used CaPs are hydroxyapatite (HA), tricalcium phosphate (TCP) and biphasic mixtures of these two. Among the TCPs,  $\beta$ -TCP and  $\alpha$ -TCP stand out for their high bioresorbability, higher than that of HA [4].  $\beta$ -TCP is a stable phase up to 1125 °C, when it turns into  $\alpha$ -TCP, which is maintained up to 1430 °C [5]. However, the transformation temperature  $\beta \rightarrow \alpha$  can be significantly altered by the presence of ionic impurities in the precursor

E-mail address: eliandra.sousa@unifesp.br (E.S. Trichês).

<sup>\*</sup> Corresponding author.

materials, which may extend up to higher temperatures [6].

Despite having good biocompatibility and high bioresorbability,  $\beta$ -TCP does not have antimicrobial activity. It is also not a bioactive biomaterial, since it does not establish a chemical connection with bone tissue, *in vivo* or *in vitro*, through the formation of an apatite layer [4,7,8,9]. It is believed that the mechanism acting at the interface of  $\beta$ -TCP with bone tissue *in vivo*, involves mechanical micro-anchoring to the tissue followed by progressive degradation through cellular processes, such as phagocytosis and cell digestion, and its replacement by healthy bone tissue [7,10].

45S5 bioglass is a bioactive glass with a molar composition of 46.1% SiO<sub>2</sub>, 24.4% Na<sub>2</sub>O, 26.9% CaO and 2.6% P<sub>2</sub>O<sub>5</sub>, being considered the gold standard in its class due to its high bioactivity [11]. Bioactive glasses are able to promote bond with bone tissue when in contact with physiological fluids (in vivo or in vitro) through the formation of an apatite layer similar to the mineral phase present in the bone [11]. Besides the high bioactivity, the 45S5 bioglass also have antimicrobial activity against some microorganisms [12,13]. Allan et al. evaluated the ability of the 45S5 bioglass to inhibit the activity of oral bacteria that commonly affect synthetic repairs of periodontal defects [12]. They found a high antimicrobial capacity of 45S5, which was associated with the release of ions from the bioglass into the medium and a consequent change in the local physiological pH. Zhang et al. evaluated the antimicrobial capacity of six bioglasses with different compositions, including 45S5 [13]. They found that all exhibited antibacterial activity for several of the bacteria tested, attributing this activity to the increase in the concentration of alkaline ions and pH of the medium.

Several studies have shown that the incorporation of bioglasses on β-TCP scaffolds can induce a significant improvement in both bioactivity and biocompatibility, but we have not found studies reporting antimicrobial properties in this composite. Hesaraki et al. prepared composites of  $\beta$ -tricalcium phosphate ( $\beta$ -TCP) and sol gel derived bioactive glass (10, 25, and 40 wt%) based on the SiO2-CaO-MgO-P2O5 system by uniaxial pressing [4]. The β-TCP/bioactive glass composites showed superior bioactivity compared to pure β-TCP, and better ability to support the growth of human osteoblastic cells. Liu et al. incorporated nano-58S bioglass produced by sol gel as a phase dispersed in β-TCP scaffolds [3]. They checked that the incorporation of nano-58S facilitated cell adhesion and proliferation and favored the formation of apatite. Lopes et al. produced porous scaffolds of  $\beta$ -TCP and  $\beta$ -TCP/BG45S5 derived from fusion by the gel casting method [14]. They also reported an improvement in cell proliferation with the addition of bioglass on the β-TCP scaffold. Like the studies cited, most β-TCP/BG scaffolds are produced from a mixture of powders of β-TCP and bioglass, the latter being produced by melting/cooling or sol gel processes with alkoxide precursors (TEOS and TEP).

The covering of inert biomaterials with bioglasses of different compositions (45S5, 58S, among others) using a sol-gel solution is a strategy that has been used to confer bioactivity and improve its biocompatibility. Mesquita-Guimarães et al. manufactured zirconia scaffolds using the replica method and covered them with 58S bioglass by immersion in a sol-gel solution [15]. The authors verified an increase in the bioactivity and cell viability of the bioinert ceramic with the bioglass coating. Haftbaradaran et al. also employed a 58S sol-gel solution to coat porous scaffolds from Vittalium, a cobalt based alloy (Co-28Cr-6Mo), verifying a significant increase in its bioactivity [16]. Yu et al. coated biocarbon scaffolds with SiO<sub>2</sub>-CaO bioglass by immersion in sol-gel solution and also verified an increase in bioactivity [17]. However, we did not find reports in the literature of the incorporation of the 45S5 bioglass (gold standard) by sol-gel solution in  $\beta$ -TCP scaffolds (bioresorbable).

In this context, this work reports for the first time the production of bioresorbable scaffolds of  $\beta\text{-TCP}$  with 45S5 bioglass incorporated from by a sol-gel solution without alkoxide precursors, with the objective of inducing a bioactive and antimicrobial behavior to  $\beta\text{-TCP}.$  The study also sought to understand the influence of the incorporation of bioglass on the crystalline structure, on the physical, mechanical, biological,

 Table 1

 Precursors used in the sol-gel synthesis of the 45S5 bioglass.

Final compound	Precursor	Content (%mol)
SiO <sub>2</sub>	H <sub>4</sub> SiO <sub>4</sub>	0,185
$P_{2}O_{5}$	$(NH_4)_3PO_4$	0,010
Na <sub>2</sub> O	NaNO <sub>3</sub>	0,098
CaO	Ca(NO <sub>3</sub> ) <sub>2</sub> .4H <sub>2</sub> O	0,110

antimicrobial properties and on the bioactivity of  $\beta$ -TCP/45S545S5 scaffolds.

# 2. Materials and methods

# 2.1. $\beta$ -TCP synthesis

β-TCP powder was synthesized by solid state reaction. Calcium phosphate (CaHPO<sub>4</sub>, Synth, 99.00%) and calcium carbonate (CaCO<sub>3</sub>, Synth, 99.00%) were mixed in a 2:1 M ratio for 30 min. Then, this mixture was calcined at 1050 °C with a heating rate of 5 °C/min and maintained for 360 min, in a muffle furnace (EDG, 3P—S). After calcination, the β-TCP powder was ground in a ball mill (Marconi, MA500) for 24 h with 6 mm diameter alumina spheres, using the weight:spheres ratio of 10:1. After grinding, the powder was analyzed by X-ray diffraction (XRD), to check the formation of the crystalline phase of β-TCP, and laser diffraction (Cilas, 1190), to control particle size.

# 2.2. $\beta$ -TCP scaffolds fabrication

 $\beta$ -TCP scaffolds were obtained using the gel casting method. The procedure used was similar to that used in other studies and is detailed below [18]. Ceramic suspensions with solids content of 30% wt. were prepared by dispersing the β-TCP powder in an aqueous solution containing 15% of the organic monomers, as hydroxymethylacrylamide (HMAM), methacrylamide (MAM) and methylenebisacrylamide (MBAM), in a 3:3:1 M ratio (HMAM:MAM:MBAM). Ammonium polyacrylate (0.5% of β-TCP mass) was added as a dispersant and the suspension was homogenized in a ball mill for 20 min. Then, a foaming agent (Lutensol ON-110, BASF) was added to the suspension (0.5% related to the suspension mass) and the suspension was agitated with a low power mixer for 3 min to produce the ceramic foam. In the sequence, it was added 2.5% related to suspension mass of initiating agent (ammonium persulfate - APS) and catalyst (tetramethylethylenediamine - TEMED) were added in 1:1 M ratio of APS:TEMED to turn the foam into a gel. The foam was poured into cylindrical molds of polyvinyl chloride (PVC) of 12 mm in diameter and 30 mm in height. The molds were maintained 24 h at room temperature (23 °C), 24 h at 70 °C and 24 h at 100  $^{\circ}$ C. The gelled foams were then demolded and submitted to the heat treatment to eliminate the monomers organic and to promote the densification of the scaffolds. The following parameters were adopted: heating from 25 to 200 °C at a rate of 5 °C/min, from 200 °C to 500 °C with 1 °C/min and maintained for 60 min, from 500 °C to 1200 °C with 5 °C/min and maintained for 120 min. After the last step, the furnace was turned off and the scaffolds were cooled into the furnace to room temperature (24 °C), without control on the cooling rate.

#### 2.3. 45S5 bioglass synthesis

45S5 bioglass (46.1 SiO $_2$ , 26.9 CaO, 24.4 Na $_2$ O, 2.6 P $_2$ O $_5$ , %mol) was synthesized by sol-gel process, without TEOS (Tetraethyl Orthosilicate, Si(OC $_2$ H $_5$ ) $_4$ ) and TEP (Triethyl phosphate, PO(C $_2$ H $_5$ ) $_3$ ), as previously described by Spirandeli et al. [19]. Briefly, the precursors listed in Table 1 were added to a beaker containing a solution of silicic acid (H $_4$ SiO $_4$ , 0.5 mol/L) under constant stirring, at 30 min intervals. At the end of the additions, a transparent bioglass sol was obtained, which was

used to impregnation the  $\beta$ -TCP scaffolds.

#### 2.4. Incorporation of 45S5 bioglass in $\beta$ -TCP scaffolds

 $\beta\text{-TCP}$  scaffolds were immersed in 200 mL of the sol-gel solution and placed in a vacuum chamber. A vacuum pressure of -1 Bar was applied and the solution was forced to fill the interior of the  $\beta\text{-TCP}$  scaffold. After 10 min under vacuum the scaffolds were removed from the solution and left for 10 min in an oven at 100 °C. This immersion and drying process was repeated three times. After the third impregnation, they were removed from the solution, dried for 24 h at 100 °C and resintered at 1200 °C, for 2 h at a heating rate of 5 °C/min for the fusion and incorporation of the bioglass in the struts. Non-impregnated  $\beta\text{-TCP}$  scaffolds were also resintered to demonstrate that the heat treatment alone did not induce changes in the crystallized phases.

#### 2.5. Characterizations

X-ray fluorescence (XRF) analyzes were performed to determine the composition of the  $\beta\text{-TCP}$  and  $\beta\text{-TCP/45S5}$  scaffolds, using an Axios MAX, PANalytical equipment. The characterization was semi-quantitative without standards with determination of chemical elements from fluorine to uranium. For the analysis, the  $\beta\text{-TCP}$  and  $\beta\text{-TCP/45S5}$  scaffolds were macerated and 10 g of each were used, which were pressed with boric acid to form the tablets. The FRX results were expressed as percentage of mass of compounds, normalized to 100%. An estimate of the percentage of glass incorporated was carried out through stoichiometric calculations, considering the silicon content, an element presents in greater quantity in the bioglass.

The morphology of the  $\beta$ -TCP and  $\beta$ -TCP/45S5 scaffolds was analyzed by scanning electron microscopy (SEM) in a TESCAN model MIRA 3 microscope operating at 10 kV. The pore size was measured in the SEM images using the Image-J software.

X-ray diffraction (XRD) analyses were performed on the  $\beta\text{-TCP}$  powder after synthesis, on the macerated  $\beta\text{-TCP}$  and  $\beta\text{-TCP}/45S5$  scaffolds (in powder form), and on the surface of the  $\beta\text{-TCP}/45S5$  scaffold (using a cylindrical sample with a diameter of 7 mm and a thickness of 2 mm). For this purpose, a model X'pert Powder diffractometer, PAN-alytical, Almelo, Holland was used. The analysis was from 20 to  $40^\circ$ , with a scan step of 10.1600 s, step size of  $0.0170^\circ$ , and CuK $\alpha$  radiation.

FT-IR analyses of macerated scaffolds (powders) were performed on a Perkin Elmer Spectrum spectrometer, Frontier model, covering the range of wave numbers from 4000 to 400 cm<sup>-1</sup> in UATR mode using a diamond crystal.

The porosity and density of the  $\beta$ -TCP and  $\beta$ -TCP/45S5 scaffolds were calculated using Eqs. (1) and (2).

$$P(\%) = \left[1 - \left(\frac{d_{Scaffolds}}{d_{teoric}}\right)\right] \times 100 \tag{1}$$

$$d_{scaffolds} = \left(\frac{m_{Scaffolds}}{V_{Scaffolds}}\right) \tag{2}$$

where,  $d_{teoric}$  is the theoretical density of  $\beta$ -TCP (3.07 g/cm<sup>3</sup>),  $m_{scaffolds}$  and  $V_{scaffolds}$  are the measured mass (g) and the calculated volume (cm<sup>3</sup>) of the scaffolds, respectively.

The compressive strength of the  $\beta$ -TCP and  $\beta$ -TCP/45S5 scaffolds was determined by uniaxial compression testing on a universal testing machine (DL2000, EMIC, 5KN load cell). The scaffolds used in this test had dimensions of 7 mm diameter and 20 mm height. To obtain statistically reliable values, 20 scaffolds were used for each group and the analysis of the experimental results was performed using the Weibull statistics, to determine the resistance and the Weibull module of the scaffolds.

#### 2.6. In vitro bioactivity assay (SBF)

The bioactivity of the  $\beta\text{-TCP}$  and  $\beta\text{-TCP}/45S5$  scaffolds was evaluated in *in vitro* tests by immersion in simulated body fluid (SBF) in a strictly controlled environment at 36.5 °C and pH of 7.40 [8]. The scaffolds remained for 12, 24, 48, 72, 120, 168, 360 and 504 h in constant linear agitation of 100 rpm, in a shaker (Julabo model SW22). The SBF solution simulates the human blood plasma inducing the mineralization of an apatite layer on the surface of bioactive materials and was prepared following the protocol developed by Kokubo and Takadama [8]. It was used in the test cylindrical samples with diameter of 7 mm and thickness of 2 mm (apparent surface area of 120 mm²). For the calculation of the SBF volume per sample, a volume ratio for a fixed surface area was used, as recommended by the ISO/FDIS standard [20], and expressed in Eq. (3).

$$V_{SBF} = \frac{S_{a-scaffold}}{10} [ml] \tag{3}$$

In the Eq. (3),  $V_{SBF}$  is the volume of SBF used e  $S_{a\text{-}scaffold}$  is the cylindrical sample superficial apparent area. This ISO standard is designed for disk-shaped samples and recommends using a higher volume than that calculated by the Eq. (3) in the test of porous samples. Thus, 30 mL of SBF was used for each sample. During the bioactivity test, the pH of the SBF solution was measured at the end of each immersion period using a pH meter (Marconi MA522) with glass electrode (AF405). There was no exchange of the SBF of the samples during the test. The mineralization of the apatite layer was verified after the test by means of XRD and SEM analyses, using the same equipments already described above.

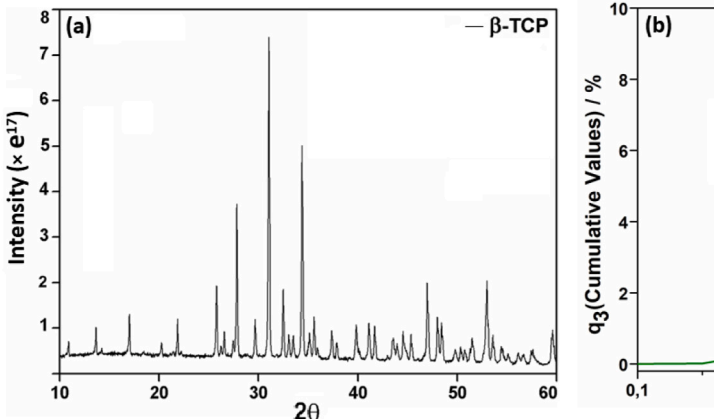
#### 2.7. In vitro biocompatibility assay

The human osteoblast cell line (MG63) was obtained from the cell bank of the Paul Ehrlich Technical Scientific Association (APABCAM, Rio de Janeiro, Brazil). The cells were cultured in Dulbecco's Modified Eagle Medium (DMEM, Cultilab, São Paulo, Brazil), supplemented with 10% fetal bovine serum (SBF, Cultilab, São Paulo, Brazil) and 100  $\mu mL$  of penicillin-streptomycin (5000 U/5000  $\mu g/mL$ ) (LGC, Biotechnology), and were kept in an oven at 37 °C in a humid atmosphere containing 5% CO2 in cell culture flasks (Kasvi, Paraná, Brazil) until about 80% confluence, the medium was changed each 48 h. After confluence, the cells were washed with phosphate-buffered saline (PBS—Cultilab) and disaggregated with 0.25% trypsin solution (Cultilab Ltda, Campinas, Brazil). The cell suspensions were centrifuged at 3000 rpm/5 min (Hermle—Z-300, Labnet, Edison, NJ, USA), and the pellet was suspended in fresh medium. MG-63 cells were seeded into a 48-well plate at a density of 1,5  $\times$  10 $^4$  cells/well per experiment.

Cell culture was used to evaluate cell viability (MTT), alkaline phosphatase activity (ALP) and total protein content (PT). These *in vitro* tests were performed in accordance with ISO-10993-5 [21] in triplicate and were performed as described by Andrade et al. [22]. All samples were subjected to ultraviolet (UV) sterilization for 30 min prior to all cell experiments. The human osteoblast cell line (MG63) was seeded and cultivated on cylindrical samples of the cut scaffolds with a diameter of 7 mm and thickness of 2 mm. Each test used five samples of  $\beta$ -TCP and  $\beta$ -TCP/45S5. The data were presented using  $\beta$ -TCP without bioglass as a control group, considering that this material have good biocompatibility [10]. The data were analyzed statistically by means of the One-way ANOVA test, considering p- value less than 0.05, and using the Graph-Pad Prism software (GraphPad Software, La Jolla California USA, www.graphpad.com).

# 2.7.1. Cell viability

Cell viability were evaluated by the 3-[4,5-dimethylthiazol-2-yl]-2,5-diphenyltetrazolium bromide (MTT) (Sigma Aldrich, Sant Louis, USA). After 3 days of cell culture on the  $\beta$ -TCP and  $\beta$ -TCP/45S5 scaffolds, quantitative assays of viable cells were conducted, through exposure to



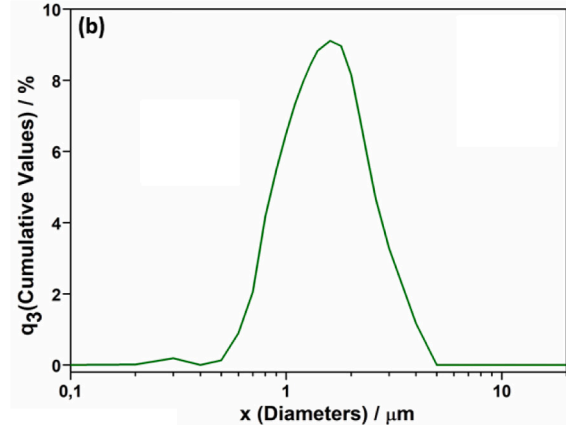


Fig. 1. (a) XRD patterns of β-TCP powder synthesized by solid state reaction, (b) Analysis of laser diffraction of β-TCP powder after synthesis and grinding.

the agent by incubation with 1 mL of MTT solution (0,5 mg/mL PBS). Spectrophotometric analysis of the dye incorporated at the 570 nm wavelength (EL808IU Biotek Instruments, Winooski, USA) was performed. Cell viability was graphically expressed as the percentage of optical density compared to the values expressed in the control group, taken as 100%.

#### 2.7.2. Total protein content (TP)

The total protein content was calculated after 10 days of culture, according to the modified Lowry method [23]. After performing the procedures, the absorbance was measured at 690 nm in a spectrophotometer (EL808IU Biotek Instruments, Winooski, USA). The protein was based entirely on a standard curve supplied from bovine albumin and expressed in  $\mu g/mL$ .

#### 2.7.3. Alkaline phosphatase activity (ALP)

The alkaline phosphatase activity was determined after 10 days of cell culture in the cell lysates of the scaffolds used to quantify the total protein, through the release of thymolphthalein by hydrolysis of the thymolphthalein monophosphate substrate, using a commercial kit according to the manufacturer's instructions (Labtest Diagnóstica). Absorbance was measured on a spectrophotometer (EL808IU Biotek Instruments, Winooski, USA) using a wavelength of 590 nm. The alkaline phosphatase activity was calculated from a standard curve using thymolphthalein on a scale from 0.012 to 0.4  $\mu$ mol of thymolphthalein/  $h/\mu g$  protein.

#### 2.8. Antimicrobial activity

The antimicrobial activity of the β-TCP and β-TCP/45S5 scaffolds was evaluated using the disk-diffusion assay on an agar plate, standardized by the M2-A8 Vol. 23, N° 1: Performance Standards for Antimicrobial Disk Susceptibility Tests; Approved Standard [24]. It was determined from the diameters of the microbial growth inhibition zones, measured under the established experimental conditions. The test was performed using Sabouraud agar (Sabouraud Dextrose Agar-Oxoid Microbiology Products) and TSA (Trypticase Soy Agar-KASVI), Tetracycline Hydrochloride (Sigma-Aldrich®) and Vancomycin Hydrochloride (Sigma-Aldrich®) as control antibiotics. Scaffolds with a diameter of 7 mm and thickness of 2 mm and control samples were tested for gram-negative (Escherichia coli, ATCC 25992), gram-positive (Staphylococcus aureus, ATCC 6538) strains and for a fungus (Candida albicans, ATCC 10231). The zones of inhibition formed were photographed and their diameters were measured using the ImageJ software. The measures were analyzed statistically by means of the One-way ANOVA test, followed by the Tukey significance test, considering p-value less than 0.05, and using the GraphPad Prism software (GraphPad Software, La Jolla

Table 2 Semi-quantitative analysis of XRF. Results expressed as percentage of mass of compounds, normalized to 100%. Other elements found in trace levels: SrO, SO<sub>3</sub>, Fe<sub>2</sub>O<sub>3</sub>, Cl, MnO, CuO, and MgO (0.18% in  $\beta$ -TCP and 0.01% in  $\beta$ -TCP/45S5).

X-ray fluorescence					
Elements	Concentration (%)				
	β-TCP scaffold	β-TCP/45S5 scaffold			
$P_{2}O_{5}$	48.6	45.0			
CaO	46.8	45.7			
$SiO_2$	0.3	4.6			
$Al_2O_3$	3.6	2.4			
Na <sub>2</sub> O	0.1	1.9			
MgO	0.2	_			
Other (SrO, SO <sub>3</sub> , Fe <sub>2</sub> O <sub>3</sub> , Cl, MnO, CuO)	0.4	0.4			

California USA, www.graphpad.com).

# 3. Results and discussion

Fig. 1(a) and (b) show the analyses of XRD and laser diffraction of the  $\beta\text{-TCP}$  powder used to manufacture the scaffolds, respectively. The powder used in the gel casting method presented only  $\beta\text{-TCP}$  crystalline phase, without any transformation into  $\alpha\text{-TCP}$  or hydroxyapatite (HA). The distribution of particle size was narrow with average particle size of 1.53  $\mu m$  (d $_{10}=0.78~\mu m$ , d $_{50}=1.42~\mu m$  and d $_{90}=2.4~\mu m$ ).

The results of the X-ray fluorescence analyses are shown in Table 2. The  $\beta\text{-TCP}$  scaffolds mostly presented the chemical elements calcium (Ca) and phosphorus (P), as denoted by the presence of the respective oxides in the analysis. A small amount of aluminum oxide (Al $_2O_3$ ) was also found, possibly from the milling process. Other oxides appear in trace levels, such as magnesium oxide (MgO), which was probably responsible for stabilizing the  $\beta\text{-TCP}$  phase at 1200 °C in the  $\beta\text{-TCP}$  scaffolds. The  $\beta\text{-TCP}/45S5$  scaffold also showed a predominance of the elements Ca and P, however a significant amount of sodium oxide (Na $_2O$ , 1.87% wt.) and silicon oxide (SiO $_2$ , 4.63% wt.). Considering the silica content (45% wt.) in the 45S5 bioglass, the stoichiometric calculations allowed to estimate that a little more than 10% of bioglass was incorporated in the  $\beta\text{-TCP}$  scaffold during the vacuum impregnation procedure.

Fig. 2(a-f) shows SEM images of the  $\beta\text{-TCP}$  and  $\beta\text{-TCP}/45S5$  scaffolds. For  $\beta\text{-TCP}$  scaffolds it is observed a bimodal pore structure with macropores uniformly distributed, in the range of 100 to 500  $\mu m$  and intragranular micropores (<1  $\mu m$ ) in the struts (indicated by circles in Fig. 2(a)). The interconnectivity between the pores is adequate to facilitate angiogenesis and promote a good vascularization, fixation, proliferation and cell differentiation, fundamental requirements for

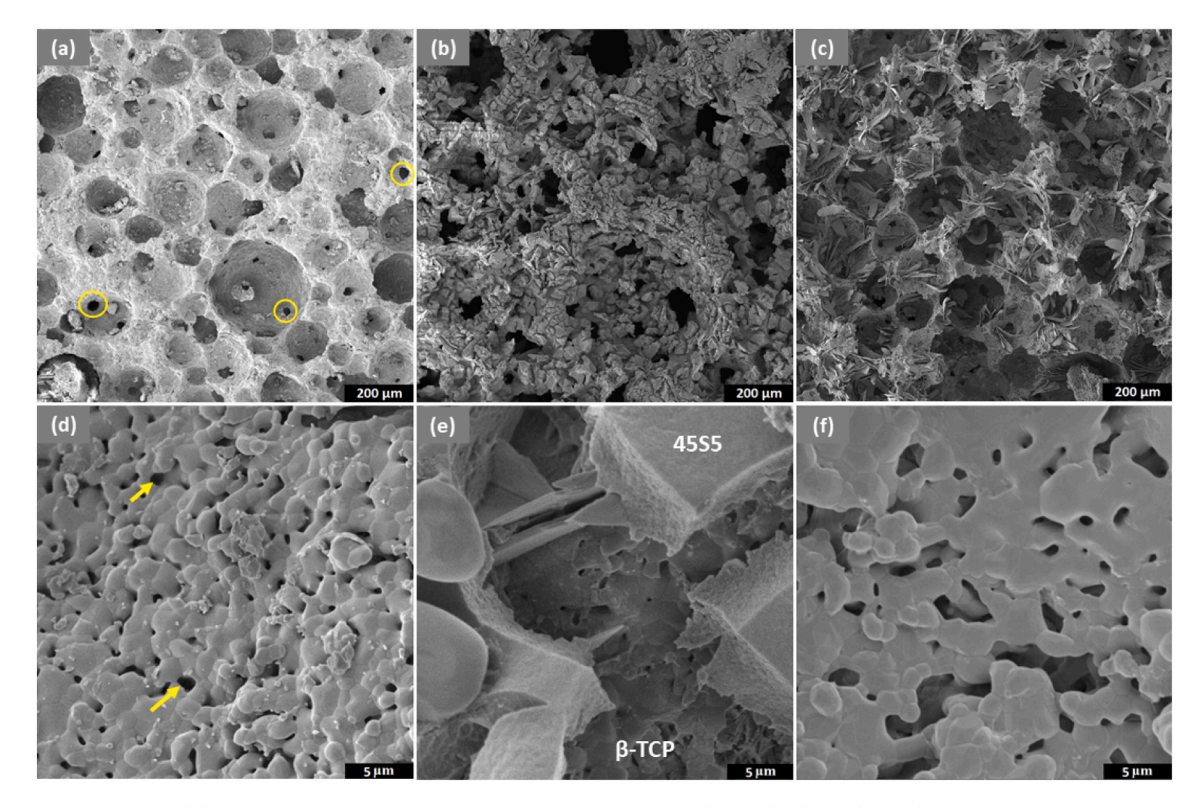


Fig. 2. SEM images of the scaffolds: (a, d)  $\beta$ -TCP, (b, e)  $\beta$ -TCP after vacuum impregnation with 45S5 bioglass sol gel solution, (c, f)  $\beta$ -TCP/45S5 after heat treatment at 1200 °C. Magnification: 250× and 10,000×.

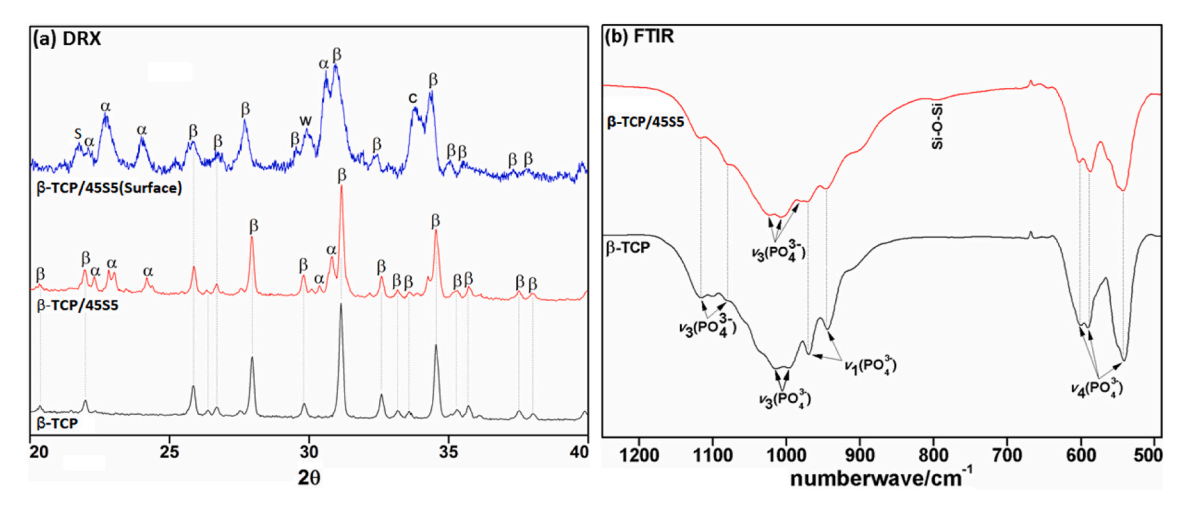


Fig. 3. (a) DRX patterns of the scaffolds:  $\beta$ -TCP,  $\beta$ -TCP/45S5 after heat treatment at 1200 °C,  $\beta$ -TCP/45S5(Surface) (surface analysis).  $\beta$ :  $\beta$ -Ca<sub>3</sub>(PO<sub>4</sub>)<sub>2</sub>  $\alpha$ :  $\alpha$ -Ca<sub>3</sub>(PO<sub>4</sub>)<sub>2</sub>; c: high-combeite, Na<sub>15.78</sub>Ca<sub>3</sub>(Si<sub>6</sub>O<sub>12</sub>); w: wollastonite, CaSiO<sub>3</sub>; S: cristobalite, SiO<sub>2</sub>. (b) FT-IR analysis using the ATR mode with powder samples from  $\beta$ -TCP and  $\beta$ -TCP/45S5 scaffolds.

bone regeneration. In turn, the microporosity found in struts plays an important role in bioactivity, especially in its interactions with proteins, in the expression of the cellular phenotype and in the osteogenesis process [25,26,27]. The micrographs of the scaffolds impregnated with bioglass (Fig. 2(b) and (e)) showed the deposition of products arising from sol gel solution on the surface of the pores, forming 45S5 xerogel plates (indicated by the arrows in Fig. 2(e)). However, for  $\beta$ -TCP/45S5 scaffolds after heat treatment at 1200 °C (Fig. 2(c) and (f)) the plates were no longer observed.

Fig. 3(a) and (b) show the XRD diffractograms and the FT-IR spectra of the  $\beta\text{-TCP}$  and  $\beta\text{-TCP}/45S5$  scaffolds, respectively. The  $\beta\text{-TCP}$  scaffold (powder) showed only peaks referring to the  $\beta\text{-TCP}$  crystalline phase

(JCPDS 00–009-0169). The absence of the  $\alpha$ –TCP phase at the employed sintering temperature (1200 °C) is probably related to the inclusion of ionic impurities in the reagents used in the synthesis, such as MgO. As reported in other studies, commercial powders (CaHPO<sub>4</sub> and CaCO<sub>3</sub>) invariably present trace levels of magnesium oxide (MgO), a potent stabilizer of the  $\beta$ -TCP phase [28,29]. The XRF analysis of the  $\beta$ -TCP scaffold showed traces of MgO, corroborating this hypothesis.

The diffractogram of the  $\beta$ -TCP/45S5 scaffold (powder) presented besides the main  $\beta$ -TCP crystalline phase, several new peaks attributed to the  $\alpha$ -TCP phase (JCPDS 00–009-0348), indicating the presence of the bioglass on the structure of the scaffold. None crystalline phase related to the crystallization of bioglass (sodium or sodium-calcium silicates)

Table 3 FT-IR bands assignment for β-TCP and β-TCP/45S5 scaffolds.

Bond	Transmittance (cm <sup>-1</sup> )	Reference
$v_1 - (PO_4^{3-})$ $v_3 - (PO_4^{3-})$	970 e 944 115, 1080, 1025, 1015, 1009, 995 e 980	[5] [32] [5] [32] [34]
ν <sub>4</sub> (PO <sub>4</sub> <sup>3-</sup> ) Si-O-Si	602, 590 e 542 800	[5] [33] [4] [30] [35]

Table 4 Values of density, porosity, compressive strength, and Weibull modulus for  $\beta$ -TCP and  $\beta$ -TCP/45S5 scaffolds.

Scaffolds	Density (g/ cm <sup>3</sup> )	Porosity (%)	Compressive strength (MPa)	Weibull modulus
β-ТСР	$0.8 \pm 0.03$	$72.4 \pm 0.9$	2.98 (2,40-3,71)	2.12 (1.48–3.04)
β-TCP/ 45S5	$0.8 \pm 0.04$	$72.9 \pm 1.3$	3.29 (2,68-4,05)	2.23 (1.57–3.17)

was found for  $\beta\text{-TCP}/45S5$ . However, in the diffractogram of the  $\beta\text{-TCP}/45S5$  scaffold analyzed without macerated ( $\beta\text{-TCP}/45S5(Surface))$ , additionally to the  $\beta\text{-TCP}$  and  $\alpha\text{-TCP}$  phases, it was observed the crystalline phases of  $Na_{15.78}Ca_3(Si_6O_{12})$  (high-combeite, JCPDS 01-078-1650), CaSiO\_3 (wollastonite, JCPDS 00-027-0088) and SiO\_2 (cristobalite, JCPDS 01-076-0940). These phases are characteristic of the crystallization of the 45S5 bioglass.

With the heat treatment at 1200 °C, the bioglass melted and diffused into the struts, inducing not only the  $\beta\to\alpha$  transformation, but also the crystallization the silicates and sodium-calcium phosphate in cooling. These phases are favorable to the bioactivity of the  $\beta$ -TCP/45S5 scaffolds. Among calcium phosphates,  $\alpha$ -TCP, in addition to being bioactive, has the highest dissolution rate and the capacity to replace with new bone [5]. Combeite and wollastonite are crystalline phases of high bioactivity, capable of inducing a strong tissue-implant connection through the formation of an apatite layer [30,31].

FT-IR spectra of the both scaffolds β-TCP and β-TCP/45S5 confirmed the predominance of bands characteristic of β-TCP [32,33]. The bands are briefly described in Table 3. Bands of the asymmetric stretching bond  $\nu_3$ –( $PO_4^{3-}$ ) (1115, 1080, 1015 e 995 cm<sup>-1</sup>), stretching bond symmetrical  $\nu_1$ –( $PO_4^{3-}$ ) (970 e 944 cm<sup>-1</sup>) and asymmetric elongation connection  $\nu_4$ –( $PO_4^{3-}$ ) (602, 590 e 542 cm<sup>-1</sup>) also were observed.

In the  $\beta$ -TCP/45S5 scaffold spectrum, some changes are noted. The bands  $\nu_1-(PO_4^{3-})$  were less intense and the 970 cm<sup>-1</sup> bands practically disappeared. A low intensity peak of the asymmetric stretching bond  $\nu_3-(PO_4^{3-})$  appeared at 980 cm<sup>-1</sup>, which can be related to the  $\alpha$ -TCP phase [34]. A new band appeared at 800 cm<sup>-1</sup> and was associated with the Si-O-Si bond of colloidal silica [35]. The peaks at 1015 and 995 cm<sup>-1</sup> found in  $\beta$ -TCP scaffold appeared displaced in  $\beta$ -TCP/45S5 to 1025 and 1009 cm<sup>-1</sup>, respectively, being attributed the bond  $\nu_3-(PO_4^{3-})$ , which is characteristic of the  $\alpha$ -TCP [5]. The other bands ( $\nu_3$  e  $\nu_4$ ) were the found in both  $\beta$ -TCP and  $\beta$ -TCP/45S5 FT-IR spectra, and they are characteristic of  $\beta$ -TCP phase. The FT-IR analysis show that the spectrum of  $\beta$ -TCP/45S5 presented several bands indicating the formation of the  $\alpha$ -TCP phase, which agrees with the XRD results.

Several studies report changes in the stability of the TCP phases due to the ion substitution promoted by Si, which reduces the thermal stability of  $\beta\text{-TCP}$  and induces the transformation to  $\alpha\text{-TCP}$  phase at temperatures lower than the theoretical ones [36]. This substitution is facilitated because the species  $PO_4{}^3\text{--}$  and  $SiO_4{}^4\text{--}$  have similar tetrahedral structures. Thus, Si enters the  $\beta\text{-TCP}$  network occupying positions of P [36]. The distinction between the  $\beta\text{-TCP}$  and  $\alpha\text{-TCP}$  FT-IR spectra is quite difficult. However, some peculiarities of the spectra can give indications and this way such analyses allow identify small differences between both phases. Besides the appearance of the peak of the Si-O-Si bond at 800 cm $^{-1}$ , there were changes in the intensities of the bands  $\nu_I$ -

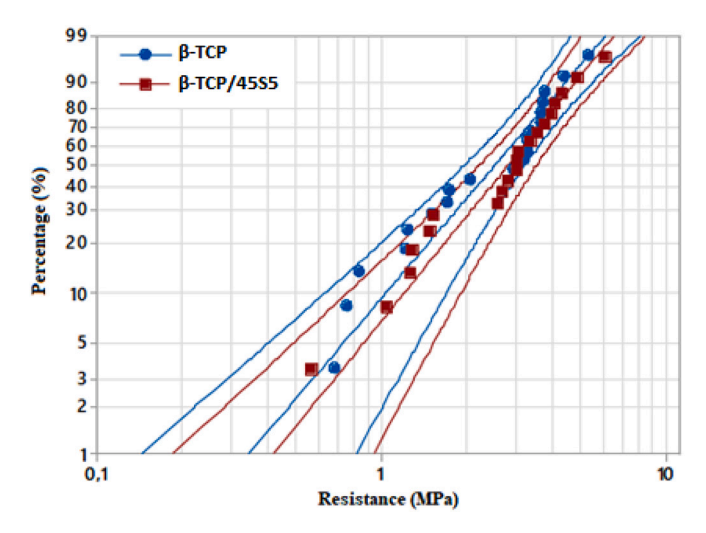


Fig. 4. Results of Weibull analysis for  $\beta$ -TCP and  $\beta$ -TCP/45S5 scaffolds.

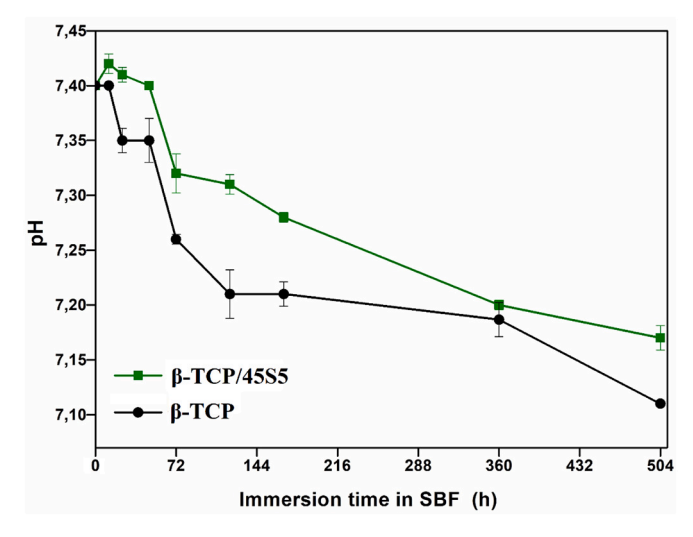


Fig. 5. Curve of the pH variation as a function of the time of immersion in SBF solution for  $\beta$ -TCP and  $\beta$ -TCP/45S5 scaffolds.

 $(PO_4^{3-})$  and the appearance of a no-intense band associated with the asymmetric elongation  $\nu_3$ - $(PO_4^{3-})$ , at 980 cm<sup>-1</sup>, which can be related to the formation of the  $\alpha$ -TCP phase.

Table 4 presents the values of density, porosity, compressive strength and Weibull modulus of the  $\beta$ -TCP and  $\beta$ -TCP/45S5 scaffolds. The  $\beta$ -TCP scaffolds showed a total porosity of 72.4  $\pm$  0.9% and density of 0.8  $\pm$  0.03 g/cm³. The incorporation of bioglass did not cause any change in the values of total porosity (72.9  $\pm$  1.3%) and density (0.8  $\pm$  0.04 g/cm³). The compressive strength and Weibull modulus values, obtained from the Weibull analysis, showed no statistical difference between the  $\beta$ -TCP and  $\beta$ -TCP/45S5 scaffolds. Before the incorporation of the bioglass, the resistance value was 2.98 (2.40–3.71) MPa, whereas in the  $\beta$ -TCP/45S5 scaffolds it was 3.29 (2.68–4.05) MPa.

These results show that the mechanical strength, density and porosity of the  $\beta$ -TCP and  $\beta$ -TCP/45S5 scaffolds are in accordance with the values reported in the literature for strength (0.1–30 MPa), density (0.05–1 g/cm³) and porosity (50–90%) of human trabecular bone [37,38,39]. Fig. 4 shows the Weibull results, expressed as the probability of failure as a function of the compressive strength (MPa) and their respective confidence intervals. It was observed the overlapping of the resistance and reliability, which indicates that the incorporation of bioglass did not cause changes in the failure mode.

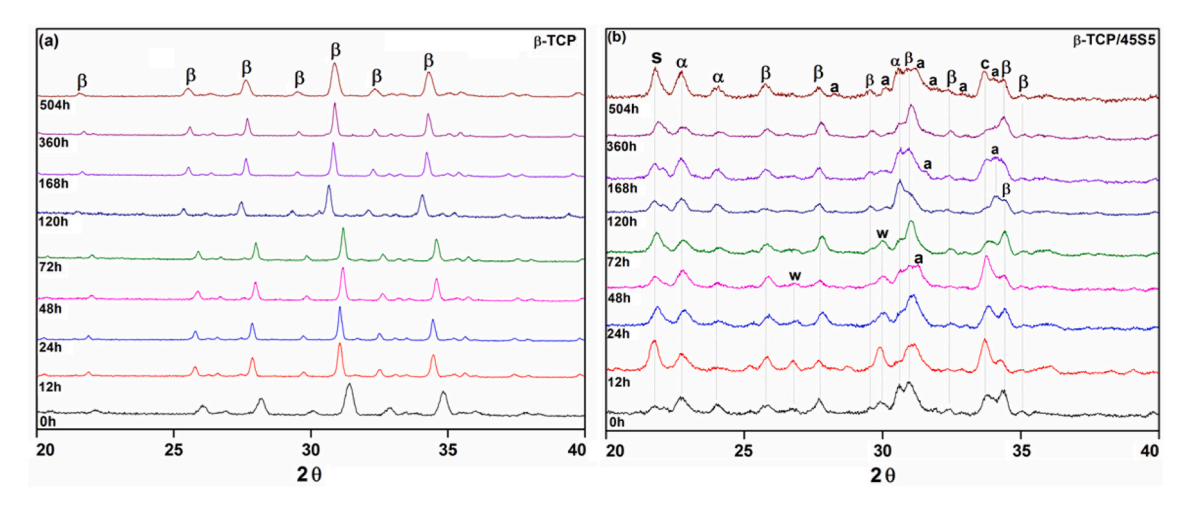


Fig. 6. XRD patterns of (a) β-TCP and (b) β-TCP/45S5 scaffolds after in vitro bioactivity assay. a: HCA-  $Ca_{10}(PO_4)_6(CO)_3$  or HA -  $Ca_{10}(PO_4)_6(OH)_2$ ; β: β- $Ca_3(PO_4)_2$  α: α- $Ca_3(PO_4)_2$ ; c: High-combeite,  $Na_{15.78}Ca_3(Si_6O_{12})$ ; w: Wollastonite,  $CaSiO_3$ ; S: Cristobalite,  $SiO_2$ .

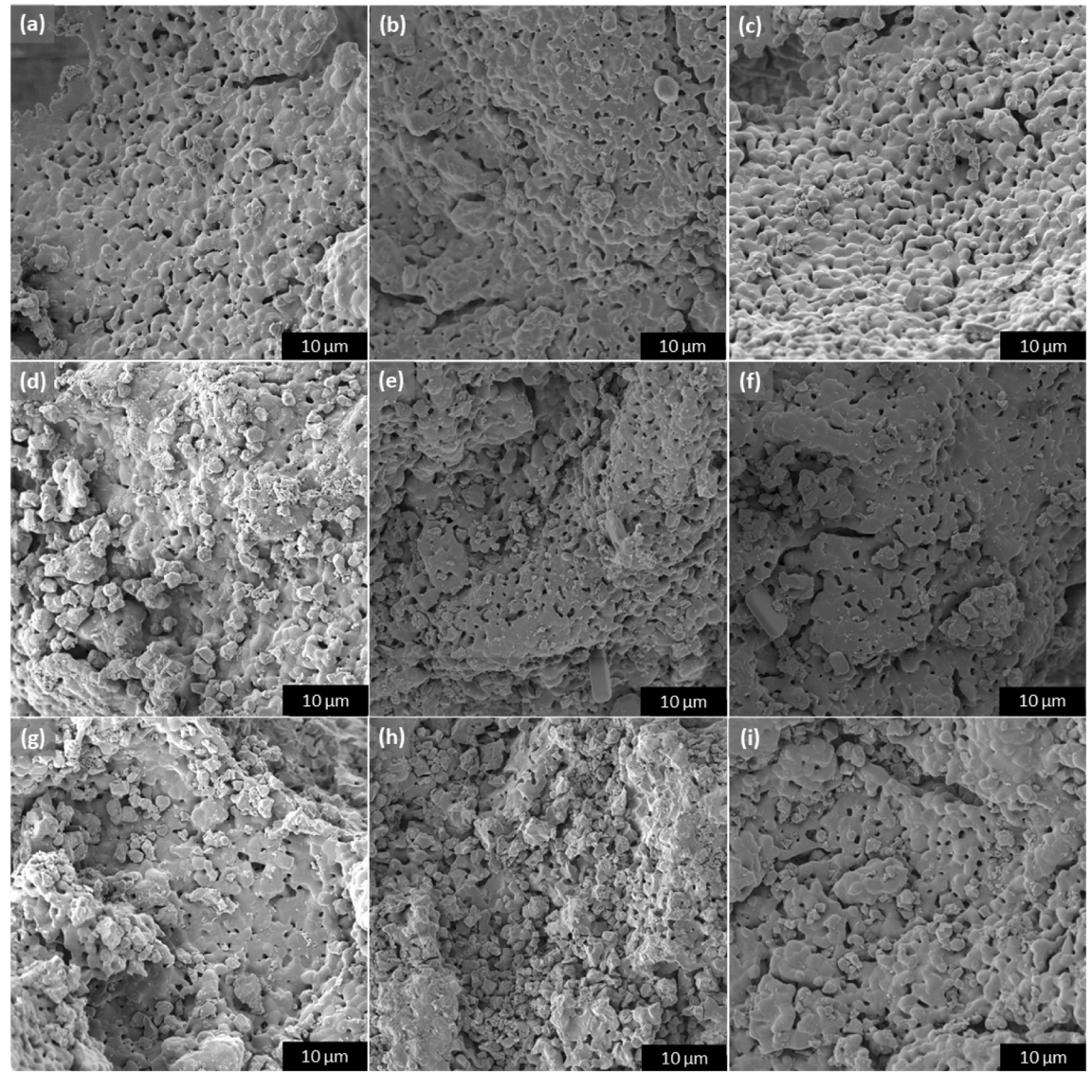


Fig. 7. SEM images of the  $\beta$ -TCP scaffolds after immersion in SBF (a) 0 h (b) 12 h (c) 24 h (d) 48 h (e) 72 h (f) 120 h (g) 168 h (h) 360 h (i) 504 h.

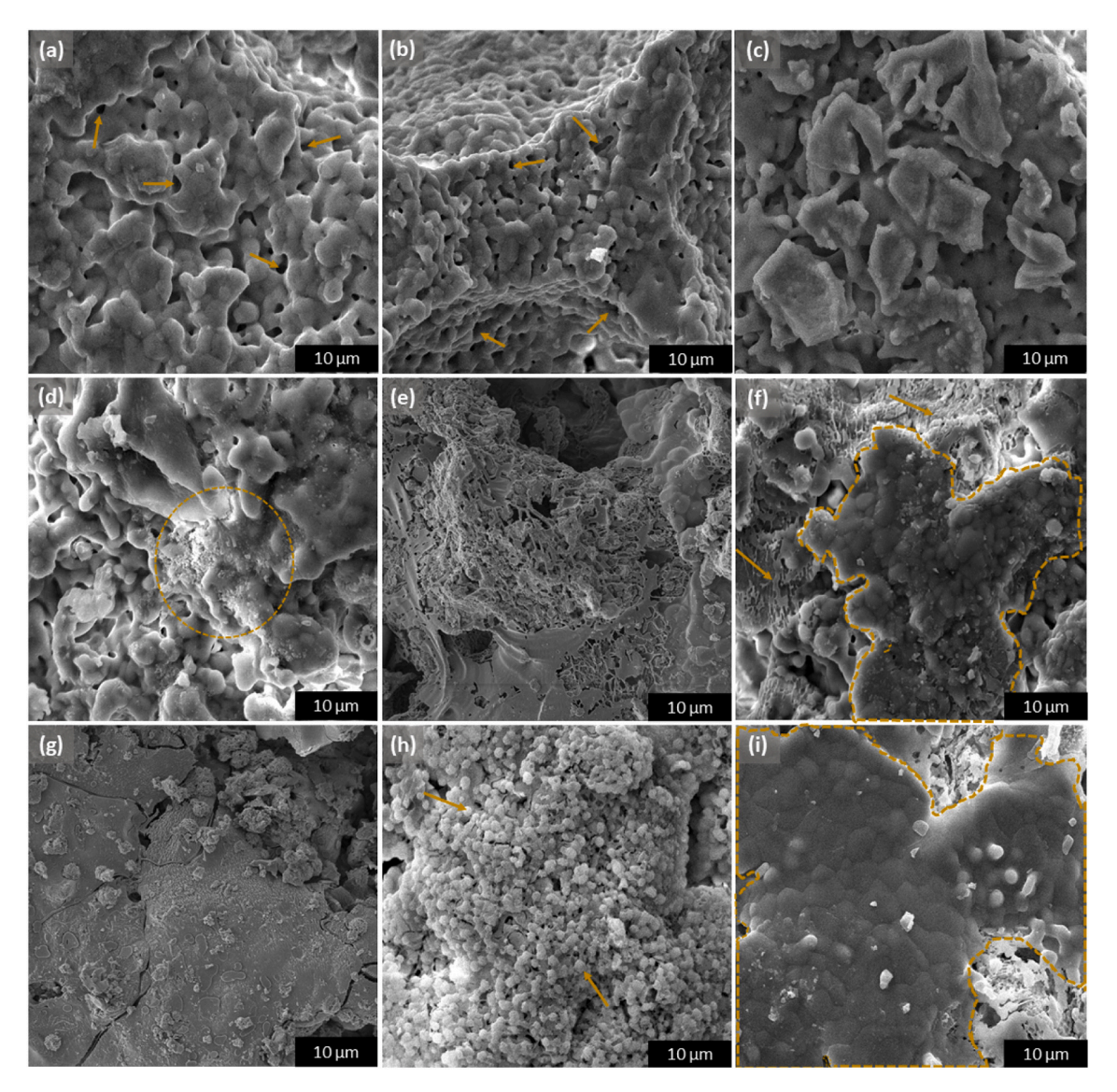


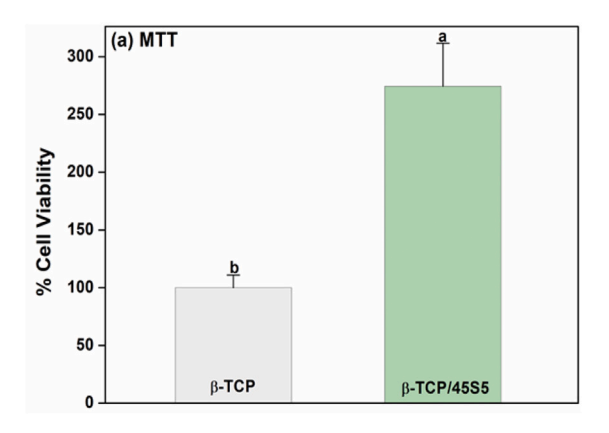
Fig. 8. SEM images of the  $\beta$ -TCP/45S5 scaffolds after immersion in SBF (a) 0 h (b) 12 h (c) 24 h (d) 48 h (e) 72 h (f) 120 h (g) 168 h (h) 360 h (i) 504 h.

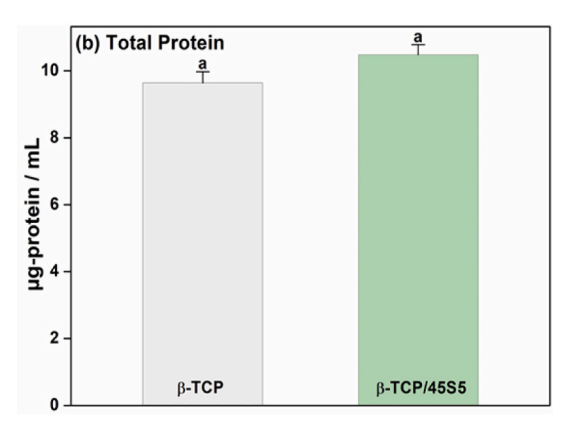
The mechanical behavior is related to the process of obtaining the composite: vacuum impregnation in the sol gel solution, fusion of the bioglass after the heat treatment at 1200 °C and slow cooling in the furnace. In the heat treatment, the  $\beta\text{-TCP}$  was partly transformed into  $\alpha\text{-TCP}$  and silicates were formed by the portion of bioglass that was not used in the polymorphic transformation  $\beta \to \alpha.$  It is known that the transformation to the  $\alpha\text{-TCP}$  phase causes microcracks in the  $\beta\text{-TCP}$  matrix due to the volumetric expansion of the unit cell and to differences in density between the  $\beta\text{-}$  and  $\alpha\text{-TCP}$  phases. Thus, it would expect a reduction in mechanical strength of the composite, as observed in other studies [1], however this did not occur. The formation of silicates, mechanically resistant phases, may also have contributed to a lesser extent to compensate for the deleterious aspect of polymorphic transformation in the resistance of  $\beta\text{-TCP}.$ 

Fig. 5 shows the curves of the pH variation as a function of the immersion time in SBF for the  $\beta$ -TCP and  $\beta$ -TCP/45S5 scaffolds. The  $\beta$ -TCP/45S5 scaffolds showed a pH value higher than that of  $\beta$ -TCP throughout the study period. In the first 12 h of immersion,  $\beta$ -TCP showed no change in pH, while in the same period  $\beta$ -TCP/45S5 showed a slight increase (7.42). Next, the pH dropped for both scaffolds, but the drop was more accented for  $\beta$ -TCP, which between 12 and 48 h reduced from 7.40 to 7.35. The decreasing trend of the curves after 12 h was maintained until the end of the test for both scaffolds.

The variation of pH with time in the  $\beta\text{-TCP}$  test presented a behavior like that observed in other studies, showing a decrease with time [1,40]. The slight increase in the pH of  $\beta\text{-TCP}/45S5$  in the first 12 h and the less accented drop with the immersion time can be attributed to the rapid release of products from the ionic dissolution of the incorporated bioglass, such as Na $^+$  and Ca $^{2+}$ , and the phase portion  $\alpha\text{-TCP}$  formed (which is more soluble than  $\beta\text{-TCP})$  [1,4,41]. The dissolution enriches the medium of these ions making it more alkaline and favoring the deposition of CaP on the surface of the scaffold.

Fig. 6 (a) and (b) shows the XRD diffractograms of  $\beta\text{-TCP}$  and  $\beta\text{-TCP}/45S5$  scaffolds after immersion in SBF. No changes in the crystalline phases were verified for  $\beta\text{-TCP}$  scaffold (Fig. 6 (a)). Conversely,  $\beta\text{-TCP}/45S5$  diffractograms (Fig. 6 (b)) showed changes over time, such as variations in intensities and dissolution of some original phases, in addition to apatite mineralization. The mineralized apatite showed a very close correspondence for carbonated hydroxyapatite, HCA,  $(Ca_{10}(PO_4)_6(CO)_3$  - JCPDS 00-035-0180) and for hydroxyapatite, HA,  $(Ca_{10}(PO_4)_3(OH)_2$  - JCPDS 00-09-0432). However, the exact identification of the mineralized phase was not possible since both phases share the same crystalline structure. In addition, it can occur the incorporation of other ions from dissolution of 45S5 in the hydroxyapatite network, preventing the accurate match of the peaks. After 48 h, the  $\beta\text{-TCP}$  peak located at 32.4° dissolved. After 168 h, the wollastonite peaks located at





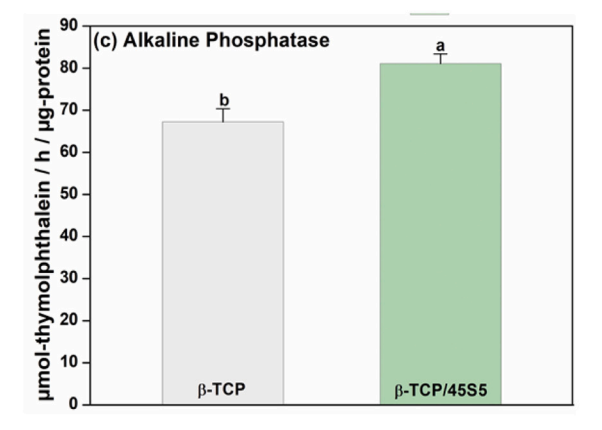


Fig. 9. In vitro biocompatibility assays for β-TCP and β-TCP/45S5 scaffolds: (a) Cell viability (Optical Density); (b) Total Protein ( $\mu$ g-Protein/mL); (c) Alkaline phosphatase ( $\mu$ mol-thymolphthalein/h/ $\mu$ g-Protein). The indices on the error bar indicate statistical differences between the samples analyzed, with a > b. A pair a-a denotes absence of statistical differences, while pair a-b indicates that the groups compared were statistically different.

 $29.9^{\circ}$  and  $25.3^{\circ}$  completely dissolve, and the formation of a peak referring to apatite. After 360 h, apatite was almost nonexistent in the diffractogram, but after 504 h new apatite peaks are found. This may indicate that the mineralization of the apatite may not have been homogeneously increased with increasing immersion times, and that the mineralized regions of the apatite may be poorly distributed on the surfaces of the scaffolds.

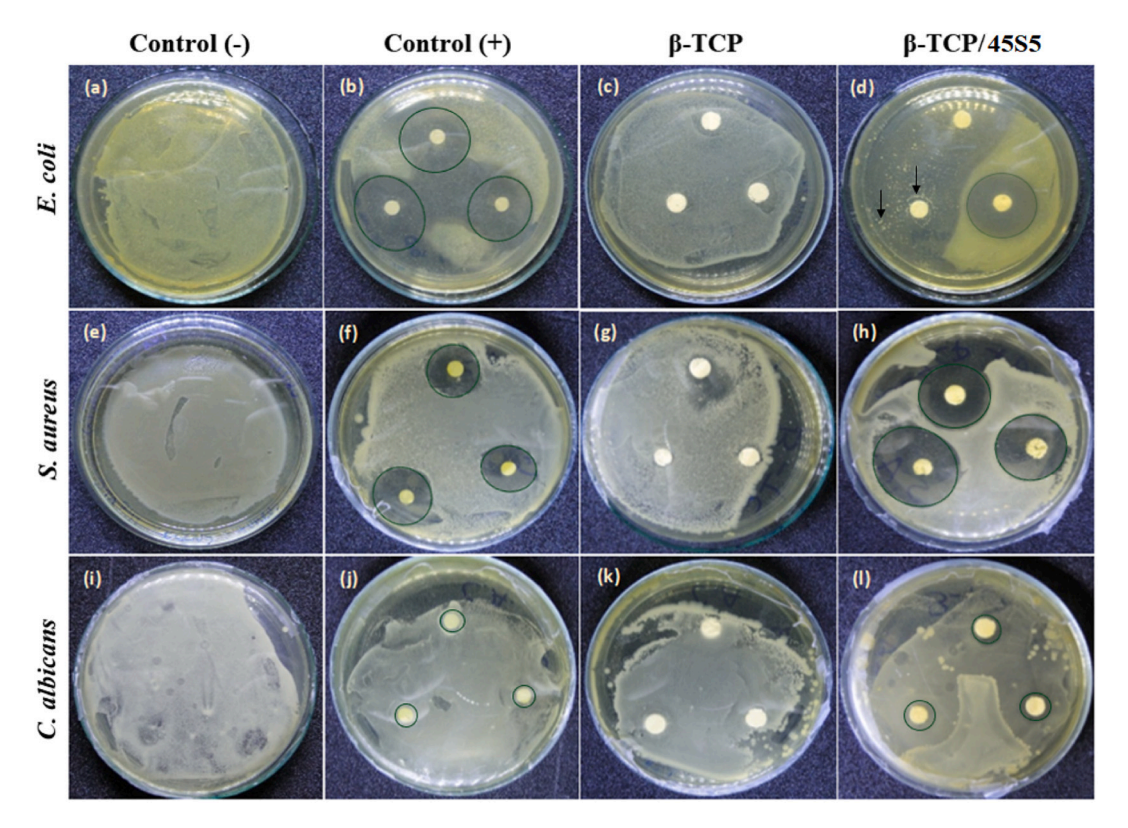
Figs. 7(a-i) and 8(a-i) show the micrographs of the  $\beta$ -TCP and  $\beta$ -TCP/45S5 scaffolds after immersion in SBF. For  $\beta$ -TCP scaffolds, there was no presence of mineralized regions on the surfaces of the struts, nor of precipitates with the characteristic morphology of the apatites, which corroborates with the XRD analyses.

Fig. 8(a-i) shows micrographs of the  $\beta$ -TCP/45S5 scaffolds after immersion in SBF. No changes in the surface were observed until 24 h of immersion. The characteristic aspect of the struts (gray areas in the micrograph) was maintained, with the micropores visible (in dark tone, indicated by the arrows in Fig. 8(a) and (b)). After 48 h of immersion, some regions with precipitates, attributed to mineralized apatite, were found in the struts of the β-TCP/45S5 scaffold, as highlighted by the circle in Fig. 8(d). In the micrograph of Fig. 8(e), after 72 h of immersion, struts presented a characteristic dissolution aspect, while the micrograph of Fig. 8(f) after 120 h and Fig. 8(g) after 168 h presents a similar aspect to that after 504 h (Fig. 8(i)), with some regions where the characteristic microporosity appears covered (as showed in the highlighted region) and others with an aspect of the beginning of mineralization (Indicated by the arrows). After 360 h, there were globular shaped nuclei deposited on the struts, as highlighted by the arrows in Fig. 8(e). After 504 h (Fig. 8(f)), regions apparently covered with the mineralized layer were found, as highlighted by the contoured region in the micrograph, where the characteristic micropores of the struts are no longer perceived.

In the same way as in XRD analyses, SEM images indicated the occurrence of mineralization but did not allow an exact relationship between the formation of apatite and the test time. The 48 h scaffolds showed more mineralization points than the 168 h, for example. Additionally, the formation of apatite does not appear to have occurred homogeneously across the surface, as several particles of mineralized globular shape can be seen in the 360 h micrograph, however practically none apatite was found in the region analyzed in the sample of X-ray diffraction.

The bioactivity the  $\beta$ -TCP/45S5 scaffolds was credited to the formation of the  $\alpha$ -TCP phase and the bioactive phases of the 45S5 on the struts. It is known that the  $\alpha$ -TCP phase can induce the formation of apatite in physiological medium, either alone or when present in  $\alpha/\beta$ -TCP composites [1,9,42]. Combeite and wollastonite are also known to induce a bioactive behavior in glass-ceramics, favoring mineralization *in vitro* and *in vivo* [26,31,30].

Fig. 9 shows the results of the biocompatibility tests for the  $\beta\text{-TCP}$  and  $\beta\text{-TCP}/45S5$  scaffolds. The results of the MTT assays (Fig. 9 (a)) indicate both scaffolds presented good cell viability, the cells were able to stick to the surface and proliferate, indicating a good interaction with the material. However, the viability for  $\beta\text{-TCP}/45S5$  was significantly higher (p<0.05), with an increase of 178% compared to  $\beta\text{-TCP}$ , and the optical density values were  $OD_{\beta\text{-TCP}}=0.11$  and  $OD_{\beta\text{-TCP}/45S5}=0.30$ , which suggests that the cells showed greater interaction and affinity with  $\beta\text{-TCP}/45S5$ . Fig. 9 (b) shows that the total protein content was only slightly higher for the  $\beta\text{-TCP}/45S5$  (approximately 8%) compared to  $\beta\text{-TCP}$ , but no statistical difference was observed (p<0.05). The results of the ALP assay (Fig. 9 (c)) showed that ALP activity was also statistically higher in cultures established on the surface of  $\beta\text{-TCP}/45S5$ 



**Fig. 10.** Photographs of Petri dishes containing (a, e, i) the samples negative control, (b, f, j) positive control, (c, g, k) β-TCP and (d, h, l) β-TCP/45S5 after disk diffusion assays in Agar against the microorganisms *E. coli, S. aureus*, and *C. albicans*. In the images, the inhibition areas are highlighted with a circle and scattered colonies are indicated with arrows.

(p < 0.05), with an increase of 13%. The behavior shown in the total protein test was consistent with the increase in activity observed in alkaline phosphatase, since both processes are related to the bone regeneration process.

The behavior verified in the biocompatibility tests can be related to the presence of Si from the bioglass, which during dissolution in the culture medium is released in the form of  $SiO_4^{4-}$ . Qiu et al. reported a significant effect of SiO<sub>4</sub><sup>4-</sup>on the process of bone formation and collagen biosynthesis and described a probable mechanism by which Si improves bone mineralization [43]. Si would act by increasing the bioactivity of prolyl 4-hydroxylase (P4H), an enzyme involved in collagen biosynthesis [44,45]. Dissolved  $SiO_4^{4-}$  enters into the cell by endocytosis or transported by a specific ion channel reaching the rough endoplasmic reticulum (RER). In the RER, P4H hydroxylates the pre-procollagen proline to hydroxyproline, an amino acid present in the collagen, forming the procollagen. In this hydroxylation an important cofactor is Fe<sup>2+</sup>, but several other cofactors may be present, such as Al<sup>3+</sup>. Thus, the Fe<sup>2+</sup> bonding site can be occupied concurrently by  $Al^{3+}$ , inhibiting P4H activity.  $SiO_4^{4-}$ can bond preferentially with  $Al^{3+}$  ions forming aluminum silicates and neutralizing the inhibition of P4H activity by Al<sup>3+</sup>, leaving Fe<sup>2+</sup> bonding sites free. Thus, it improves bone mineralization, collagen synthesis and alkaline phosphatase activity [43,44].

The antimicrobial activity of the  $\beta$ -TCP and  $\beta$ -TCP/45S5 scaffolds was assessed through measurements of the mean diameters of the inhibition halos formed in the disk diffusion test, shown in Fig. 10. The negative controls (–) of the three microorganisms (Fig. 10 (a), (e) and (i)) indicated that microbial cultures attach and proliferated, covering the entire plate with a thick microbial film. Positive control samples (+) tested for bacteria and the fungus showed inhibition of the growth of microorganisms, as shown by the inhibition halos formed (Fig. 10 (b), (f) and (j)).  $\beta$ -TCP did not show growth inhibition of any of the tested microorganisms. The growth of the cultures occurred without any impediment, being comparable to the result obtained by the tests of the

negative controls, as shown in Fig. 10 (c), (g) and (k). Already  $\beta$ -TCP/45S5 was able to create an inhibition zone comparable to positive control, preventing the proliferation of *E. coli* (Fig. 10 (d)), *S. aureus* (Fig. 10 (h)) and *C. albicans* (Fig. 10 (l)).

The measurements of the diameters of the inhibition halos formed in the assay are shown in the graphs of Fig. 11. The results obtained from the Tukey test and expressed in the graphs showed that there was no statistical difference between the  $\beta$ -TCP/4SS5 scaffolds and the positive control (p < 0.05) in the test against *E. coli* (Fig. 11 (a)). On the other hand, the inhibition presented by  $\beta$ -TCP/4SS5 was statistically higher than that of the positive control (p < 0.05) for both *S. aureus* and *C. albicans*. Thus, the microorganisms tested were susceptible to the  $\beta$ -TCP/4SS5 scaffolding, with antimicrobial activity equal to or greater than that of antibiotics and antifungals commonly used to combat microbial infections.

These results indicate that the incorporation of the 45S5 bioglass in the β-TCP scaffolds induced an antimicrobial behavior that does not exist in pure β-TCP, preventing the fixation and proliferation of the tested microorganisms. This behavior can be attributed to the release of ionic species from bioglass in the test medium and the consequent increase in local pH. The change in pH can induce changes in osmotic pressure, alter the integrity of the cytoplasmic membrane and cause denaturation of proteins, affecting intracellular functions, such as the activity of enzymes, that are essential to the cellular metabolism of the microorganism [46,47]. Echezarreta-López et al. [48] proposed a mechanism of action antimicrobial the bioglass described in three stages: (1) ionic release, (2) increased osmolarity and (3) increased local pH. These phenomena interfere with the bacterial intracellular ionic balance, which results in depolarization of the cell membrane and its subsequent disruption. In addition, residuals from the bioglass dissolved in the medium can also get in contact direct with the microorganisms, damaging the cell walls [47].

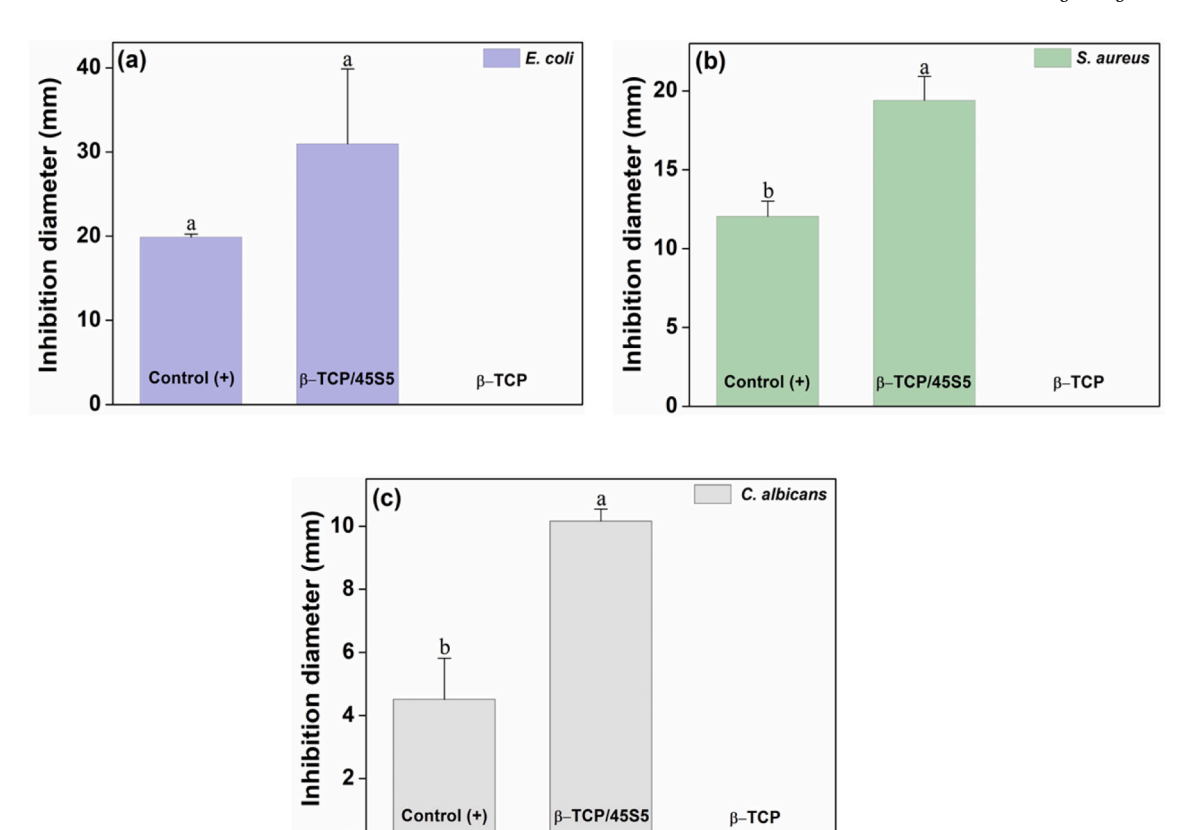


**Fig. 11.** Inhibition diameters measured in samples against: (a) *E. coli*; (b) *S. aureus* and (c) *C. albicans*. The indices on the error bar indicate statistical differences between the samples analyzed by the Tukey test (p < 0.05), with a > b. A pair a-a denotes no statistical difference, while pair a-b indicates that the groups compared were statistically different.

# 4. Conclusion

Bioresorbable β-TCP scaffolds with incorporated 45S5 bioglass by sol gel process were successfully obtained by the procedure presented in this work. The scaffolds produced by the gel casting method showed total porosity of 72% and macrostructure with open and interconnected pores. The incorporation of the 45S5 bioglass induced the partial transformation of  $\beta$ -TCP into  $\alpha$ -TCP as well as the crystallization of highly bioactive calcium and sodium-calcium silicates. Despite the formation of the  $\alpha$ -TCP phase, there was no decrease in the mechanical strength or in the Weibull modulus values, suggesting that the bioglass acted by improving the bonding strength of the β-TCP grains. Also, the presence of 45S5 conferred bioactivity, inducing the formation of an apatite layer on the  $\beta$ -TCP/45S5 scaffold that was not found in the  $\beta$ -TCP scaffold, in addition to increased biocompatibility, as indicated by in vitro biocompatibility tests. This increase was related to the dissolution of ionic species from the incorporated bioglass, mainly silicon, which neutralizes the inhibition of the activity of the enzyme prolyl 4-hydroxylase. Ionic dissolution also leads to a rise in the pH of the medium, contributing to the apatite mineralization in SBF and to the inhibition of microbial growth (disk diffusion tests), since the tested microorganisms are susceptible changes in the pH of the medium. The biocompatibility tests showed an increase of cell viability number, and better activity and osteoblast differentiation in MG63. Thus, the β-TCP/45S5 scaffold presented a set of very promising properties and it can be considered a potential candidate for application in bone tissue engineering.

#### CRediT authorship contribution statement

Martins, E, F. and Esposito, E. contributed to the preparation and execution of the antimicrobial tests, with the statistical analyzes

performed and with the final review of the article;

Ribas R. G., Campos, T. M. B. and Thim, G. P. contributed to the elaboration and execution of the bioglass synthesis, with the chemical, morphological and structural characterizations (FRX, SEM and DRX), with the statistical analyzes carried out and with the final review of the article;

Vasconcellos, L. M. R.e Amaral, S. S. contributed to the elaboration and execution of *in vitro* biocompatibility assays (MTT, PT and ALP) and to the final review of the article;

Spirandeli, B. R. was the main author of the work and Trichês, E. S. the research supervisor.

### **Declaration of competing interest**

The authors declare that they have no known competing financial interests or personal relationships that could have appeared to influence the work reported in this paper.

#### Acknowledgments

The authors are grateful to São Paulo Research Foundation – FAPESP (2015/24659-7) for the financial support. Also, the authors are grateful to the Brazilian agencies: Coordination for the Improvement of Higher Education Personnel - CAPES and São Paulo Research Foundation, FAPESP for the scholarship granted to Spirandeli, B.R. (project  $n^{\circ}$  2.430921/2019-01, CAPES), Ribas R.G. (project  $n^{\circ}$  27079-7/2017, FAPESP) and Martins, E.F. (project  $n^{\circ}$  7.500613/2020-00, CAPES).

#### References

[1] L. Xie, H. Yu, Y. Deng, W. Yang, L. Liao, Q. Long, Preparation, characterization and in vitro dissolution behavior of porous biphasic  $\alpha/\beta$ -tricalcium phosphate

- bioceramics, Mater. Sci. Eng. C 59 (2016) 1007–1015, https://doi.org/10.1016/j.
- [2] S.V. Dorozhkin, Bioceramics of calcium orthophosphates, Biomaterials. 31 (2010) 1465–1485, https://doi.org/10.1016/j.biomaterials.2009.11.050.
- [3] J. Liu, C. Gao, P. Feng, S. Peng, C. Shuai, Selective laser sintering of β-TCP/nano-58S composite scaffolds with improved mechanical properties, Mater. Des. 84 (2015) 395–401, https://doi.org/10.1016/j.matdes.2015.06.161.
- [4] S. Hesaraki, M. Safari, M.A. Shokrgozar, Development of beta-tricalcium phosphate/sol-gel derived bioactive glass composites: physical, mechanical, and in vitro biological evaluations, J Biomed Mater Res B Appl Biomater 91 (2009) 459–469, https://doi.org/10.1002/jbm.b.31422.
- [5] R.G. Carrodeguas, S. de Aza, α-Tricalcium phosphate: synthesis, properties and biomedical applications, Acta Biomater. 7 (2011) 3536–3546, https://doi.org/ 10.1016/j.actbio.2011.06.019.
- [6] M. Motisuke, R. García Carrodeguas, C.A.C. Zavaglia, Mg-free precursors for the synthesis of pure phase Si-doped α-Ca<sub>3</sub>(PO4)<sub>2</sub>, Key Eng. Mater. 361–363 (2007) 199–202. doi:https://doi.org/10.4028/www.scientific.net/kem.361-363.199.
- [7] S. Kotani, Y. Fujita, T. Kitsugi, T. Nakamura, T. Yamamuro, C. Ohtsuki, T. Kokubo, Bone bonding mechanism of beta-tricalcium phosphate, J. Biomed. Mater. Res. 25 (1991) 1303–1315, https://doi.org/10.1002/jbm.820251010.
- [8] T. Kokubo, H. Takadama, How useful is SBF in predicting in vivo bone bioactivity? Biomaterials. 27 (2006) 2907–2915, https://doi.org/10.1016/j. biomaterials.2006.01.017.
- [9] R. Xin, Y. Leng, J. Chen, Q. Zhang, A comparative study of calcium phosphate formation on bioceramics in vitro and in vivo, Biomaterials (2005), https://doi. org/10.1016/j.biomaterials.2005.04.028.
- [10] A. Ogose, N. Kondo, H. Umezu, T. Hotta, H. Kawashima, K. Tokunaga, T. Ito, N. Kudo, M. Hoshino, W. Gu, N. Endo, Histological assessment in grafts of highly purified beta-tricalcium phosphate (OSferion®) in human bones, Biomaterials. 27 (2006) 1542–1549, https://doi.org/10.1016/j.biomaterials.2005.08.034.
- [11] J.R. Jones, Reprint of: review of bioactive glass: from Hench to hybrids, Acta Biomaterialia (2015), https://doi.org/10.1016/j.actbio.2015.07.019.
- [12] I. Allan, H. Newman, M. Wilson, Antibacterial activity of particulate Bioglass® against supra- and subgingival bacteria, Biomaterials. 22 (2001) 1683–1687, https://doi.org/10.1016/S0142-9612(00)00330-6.
- [13] D. Zhang, O. Leppäranta, E. Munukka, H. Ylänen, M.K. Viljanen, E. Eerola, M. Hupa, L. Hupa, Antibacterial effects and dissolution behavior of six bioactive glasses, Journal of Biomedical Materials Research - Part A. 93 (2010) 475–483, https://doi.org/10.1002/jbm.a.32564.
- [14] J.H. Lopes, J.A. Magalhães, R.F. Gouveia, C.A. Bertran, M. Motisuke, S.E. A. Camargo, E. de S. Trichês, Hierarchical structures of ??-TCP/45S5 bioglass hybrid scaffolds prepared by gelcasting, J. Mech. Behav. Biomed. Mater. (2016), https://doi.org/10.1016/j.imbbm.2016.04.028.
- [15] J. Mesquita-Guimarães, L. Ramos, R. Detsch, B. Henriques, M.C. Fredel, F.S. Silva, A.R. Boccaccini, Evaluation of in vitro properties of 3D micro-macro porous zirconia scaffolds coated with 58S bioactive glass using MG-63 osteoblast-like cells, J. Eur. Ceram. Soc. 39 (2019) 2545–2558, https://doi.org/10.1016/j.ieurceramsoc.2019.01.029
- [16] M. Haftbaradaran-Esfahani, M. Ahmadian, A. Nassajpour-Esfahani, Fabrication and characterization of porous biomedical Vitallium alloy with 58S bioglass coating prepared by sol-gel method, Appl. Surf. Sci. 506 (2020), 144959, https://doi.org/ 10.1016/j.apsusc.2019.144959.
- [17] M. Yu, E. Fiume, E. Verné, T. Saunders, M.J. Reece, F. Baino, Bioactive sol-gel glass-coated wood-derived biocarbon scaffolds, Mater. Lett. 232 (2018) 14–17, https://doi.org/10.1016/j.matlet.2018.08.067.
- [18] L. Siqueira, C.G. De Paula, M. Motisuke, R.F. Gouveia, S.E.A. Camargo, N.V. M. Milhan, E.S. Trichès, Preparation, Characterization and biological studies of B-TCP and B-TCP/Al2O3 scaffolds obtained by gel-casting of foams, Mater. Res. 20 (2017) 973–983, https://doi.org/10.1590/1980-5373-MR-2016-0467.
- [19] B.R. Spirandeli, T.M.B. Campos, R.G. Ribas, G.P. Thim, E.S. Trichês, Evaluation of colloidal and polymeric routes in sol-gel synthesis of a bioactive glass-ceramic derived from 45S5 bioglass, Ceram. Int. (2020) 0–1, https://doi.org/10.1016/j. ceramint.2020.05.108.
- [20] International Organization for Standardization, ISO 23317:2014 implants for surgery, in: Vitro Evaluation for Apatite-Forming Ability of Implant Materials, 2014.
- [21] International Organization for Standardization, Biological evaluation of medical devices (ISO 10993-5), 2009.
- [22] D.P. de Andrade, L.M.R. de Vasconcellos, I.C. Silva Carvalho, L.F. de Brito Penna Forte, E.L. de Souza Santos, R.F. do Prado, D.R. dos Santos, C.A. Alves Cairo, Y. R. Carvalho, Titanium-35niobium alloy as a potential material for biomedical implants: in vitro study, Mater. Sci. Eng. C 56 (2015) 538–544, https://doi.org/ 10.1016/j.msec.2015.07.026.
- [23] Lowry O.H., N.J. Rosebrough, Farr A.L., R.J. Randall, Protein measurement with the Folin phenol reagent, J. Biol. Chem. (1951), https://doi.org/10.1016/0922-22020/002010.
- [24] M.P. Weinstein, M02 performance standards for antimicrobial disk susceptibility tests, 13th Edition, 2018. https://clsi.org/standards/products/microbiology/do cuments/m02/
- [25] S. Sánchez-Salcedo, F. Balas, I. Izquierdo-Barba, M. Vallet-Regí, In vitro structural changes in porous HA/β-TCP scaffolds in simulated body fluid, Acta Biomater. 5 (2009) 2738–2751, https://doi.org/10.1016/j.actbio.2009.03.025.
- [26] V.P. Galván-Chacón, S. Eqtesadi, A. Pajares, P. Miranda, F. Guiberteau, Elucidating the role of 45S5 bioglass content in the density and flexural strength of robocast

- β-TCP/45S5 composites, Ceram. Int. 44 (2018) 12717–12722, https://doi.org/10.1016/j.ceramint.2018.04.074.
- [27] L.-C. Gerhardt, A.R. Boccaccini, Bioactive glass and glass-ceramic scaffolds for bone tissue engineering, Materials. 3 (2010) 3867–3910, https://doi.org/10.3390/ ma3073867
- [28] R. Enderle, F. Götz-Neunhoeffer, M. Göbbels, F.A. Müller, P. Greil, Influence of magnesium doping on the phase transformation temperature of β-TCP ceramics examined by Rietveld refinement, Biomaterials. 26 (2005) 3379–3384, https://doi. org/10.1016/j.biomaterials.2004.09.017.
- [29] J.W. Reid, K. Fargo, J.A. Hendry, M. Sayer, The influence of trace magnesium content on the phase composition of silicon-stabilized calcium phosphate powders, Mater. Lett. 61 (2007) 3851–3854, https://doi.org/10.1016/j.matlet.2006.12.046.
- [30] I. Cacciotti, M. Lombardi, A. Bianco, A. Ravaglioli, L. Montanaro, Sol-gel derived 45S5 bioglass: synthesis, microstructural evolution and thermal behaviour, J. Mater. Sci. Mater. Med. 23 (2012) 1849–1866, https://doi.org/10.1007/s10856-012-4667-6
- [31] J.A. Juhasz, S.M. Best, W. Bonfield, M. Kawashita, N. Miyata, T. Kokubo, T. Nakamura, Apatite-forming ability of glass-ceramic apatite-wollastonite polyethylene composites: effect of filler content, J. Mater. Sci. Mater. Med. 14 (2003) 489–495, https://doi.org/10.1023/A:1023499728588.
- [32] G. Tripathi, K. Ishikawa, Materials Science & Engineering C Fabrication and in vitro dissolution evaluation of low-crystalline β-TCP blocks through aqueous I, Materials Science & Engineering C. 101 (2019) 228–231, https://doi.org/10.1016/ i.msec.2019.03.106
- [33] A. Jillavenkatesa, R.A. Condrate, The infrared and raman spectra of β- and α-tricalcium phosphate (Ca3(PO4)2), Spectrosc. Lett. 31 (1998) 1619–1634, https://doi.org/10.1080/00387019808007439.
- [34] M. Sayer, A.D. Stratilatov, J. Reid, L. Calderin, M.J. Stott, X. Yin, M. MacKenzie, T. J.N. Smith, J.A. Hendry, S.D. Langstaff, Structure and composition of silicon-stabilized tricalcium phosphate, Biomaterials. 24 (2003) 369–382, https://doi.org/10.1016/S0142-9612(02)00327-7.
- [35] C. Hollenstein, A.A. Howling, C. Courteille, D. Magni, S.M. Scholz, G.M. W. Kroesen, N. Simons, W. de Zeeuw, W. Schwarzenbach, Silicon oxide particle formation in RF plasmas investigated by infrared absorption spectroscopy and mass spectrometry, J. Phys. D. Appl. Phys. 31 (1998) 74–84, https://doi.org/10.1088/0022-3727/31/1/011.
- [36] J.W. Reid, A. Pietak, M. Sayer, D. Dunfield, T.J.N. Smith, Phase formation and evolution in the silicon substituted tricalcium phosphate/apatite system, Biomaterials. 26 (2005) 2887–2897, https://doi.org/10.1016/j. biomaterials.2004.09.005.
- [37] V. Karageorgiou, D. Kaplan, Porosity of 3D biomaterial scaffolds and osteogenesis, Biomaterials. 26 (2005) 5474–5491, https://doi.org/10.1016/j. biomaterials.2005.02.002.
- [38] Handbook of Biomaterial Properties, 1998. doi:https://doi.org/10.1007/978-1-46 15-5801-9.
- [39] T. Almela, I.M. Brook, K. Khoshroo, M. Rasoulianboroujeni, F. Fahimipour, M. Tahriri, E. Dashtimoghadam, A. El-Awa, L. Tayebi, K. Moharamzadeh, Simulation of cortico-cancellous bone structure by 3D printing of bilayer calcium phosphate-based scaffolds, Bioprinting. 6 (2017) 1–7, https://doi.org/10.1016/j. https://doi.org/10.1016/j.
- [40] Y. Yang, Y. Zhao, G. Tang, H. Li, X. Yuan, Y. Fan, In vitro degradation of porous poly(I-lactide-co-glycolide)/β-tricalcium phosphate (PLGA/β-TCP) scaffolds under dynamic and static conditions, Polym. Degrad. Stab. 93 (2008) 1838–1845, https://doi.org/10.1016/j.polymdegradstab.2008.07.007.
- [41] S. Cai, G.H. Xu, X.Z. Yu, W.J. Zhang, Z.Y. Xiao, K.D. Yao, Fabrication and biological characteristics of β-tricalcium phosphate porous ceramic scaffolds reinforced with calcium phosphate glass, J. Mater. Sci. Mater. Med. 20 (2009) 351–358, https://doi.org/10.1007/s10856-008-3591-2
- [42] P. Velasquez, Z.B. Luklinska, L. Meseguer-Olmo, J.E. Mate-Sanchez De Val, R. A. Delgado-Ruiz, J.L. Calvo-Guirado, M.P. Ramirez-Fernandez, P.N. de Aza, αtCP ceramic doped with dicalcium silicate for bone regeneration applications prepared by powder metallurgy method: in vitro and in vivo studies, Journal of Biomedical Materials Research Part A. 101 A (2013) 1943–1954, https://doi.org/10.1002/jbm.a.34495.
- [43] Z.Y. Qiu, I.S. Noh, S.M. Zhang, Silicate-doped hydroxyapatite and its promotive effect on bone mineralization, Front. Mater. Sci. 7 (2013) 40–50, https://doi.org/ 10.1007/s11706-013-0193-9.
- [44] D.M. Reffitt, N. Ogston, R. Jugdaohsingh, H.F.J. Cheung, B.A.J. Evans, R.P. H. Thompson, J.J. Powell, G.N. Hampson, Orthosilicic acid stimulates collagen type 1 synthesis and osteoblastic differentiation in human osteoblast-like cells in vitro, Bone. 32 (2003) 127–135, https://doi.org/10.1016/S8756-3282(02)00950-X.
- [45] J.D. Birchall, The essentiality of silicon in biology, Chem. Soc. Rev. (1995), https://doi.org/10.1039/CS9952400351.
- [46] A.A. Ahmed, A.A. Ali, D.A.R. Mahmoud, A.M. El-Fiqi, Preparation and characterization of antibacterial P2O 5-CaO-Na2O-Ag2O glasses, Journal of Biomedical Materials Research - Part A. 98 A (2011) 132–142, https://doi.org/ 10.1002/jbm.a.33101.
- [47] S. Hu, J. Chang, M. Liu, C. Ning, Study on antibacterial effect of 4585 Bioglass®, J. Mater. Sci. Mater. Med. 20 (2009) 281–286, https://doi.org/10.1007/s10856-008 2564 5
- [48] M.M. Echezarreta-López, M. Landin, Using machine learning for improving knowledge on antibacterial effect of bioactive glass, Int. J. Pharm. 453 (2013) 641–647, https://doi.org/10.1016/j.ijpharm.2013.06.036.